Theor Chem Acc (2010) 127:345–354
DOI 10.1007/s00214-009-0723-9

REGULAR ARTICLE

Enhanced detonation sensitivities of silicon analogs of PETN: reaction force analysis and the role of σ–hole interactions

Jane S. Murray · Pat Lane · Anian Nieder · Thomas M. Klapötke · Peter Politzer

Received: 19 November 2009 / Accepted: 18 December 2009 / Published online: 12 January 2010

Abstract Si-pentaerythritol tetranitrate (PETN), $Si[CH_2ONO_2]_4$, is a silicon analog of the widely used explosive PETN, $C[CH_2ONO_2]_4$. Si-PETN is extremely sensitive to impact, much more so than PETN. This was attributed by Liu et al. to Si-PETN having a much lower activation barrier to decomposition, via a facile rearrangement that is not as readily available to PETN, and which releases considerable energy that can promote further steps. We have investigated computationally why the barrier to the rearrangement is so much lower for Si-PETN than for PETN, using **5**, $(H_3C)_3C–CH_2ONO_2$, and **6**, $(H_3C)_3Si–CH_2ONO_2$, as models for PETN and Si-PETN. Reaction force analysis shows that most of the difference between the rearrangement barriers for **5** and **6** comes about in the initial (reactant) stages of the processes, in which **6** benefits from a 1,3 electrostatic interaction involving a positive σ–hole on the silicon and the negative linking oxygen. The analogous interaction is weaker in **5**, since the central carbon does not have positive σ–holes; furthermore, this carbon is less able than silicon to temporarily expand its coordination sphere. A similar explanation involving a positive silicon σ–hole and a linking oxygen is proposed for Si-PETN. The greater exothermicity of the rearrangement of **6** (and also Si-PETN) can be rationalized, following Liu et al., in terms of the formation of the strong Si–O bond.

Keywords PETN · Si-PETN · Reaction force · Silicon–oxygen interactions · σ–Hole interactions · Impact sensitivities · Nitrate esters · Energetic molecules

1 PETN and Si-PETN

Pentaerythritol tetranitrate (PETN, **1**) is a well-known energetic compound, in the category of nitrate esters. It can be prepared by reacting the corresponding tetrol with nitric acid [1]. PETN has two polymorphs [2], the less common (PETN II) occurring above 130 °C. Our focus shall be solely upon PETN I. It has a crystal density of 1.778 g/cm^3 at 22 °C, with two molecules per unit cell [2].

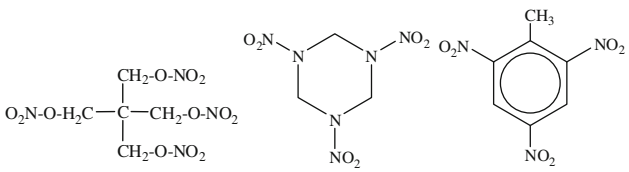

1 **2** **3**

PETN has good detonation velocity and pressure, slightly below those of RDX (**2**) but well above TNT (**3**) [3]. It has been used extensively in blasting cap fillings, detonation cords, demolition devices, industrial explosives, etc. [3, 4]. However, PETN is quite sensitive to impact, more so than RDX and much more than TNT; the required

J. S. Murray (✉) · P. Lane · P. Politzer
Department of Chemistry, University of New Orleans, New Orleans, LA 70148, USA
e-mail: jsmurray@uno.edu

A. Nieder · T. M. Klapötke
Department of Chemistry and Biochemistry, Ludwig-Maximilian University of Munich, Butenandtstr. 5-13(D), 81377 Munich, Germany

T. M. Klapötke
Departments of Mechanical Engineering and Chemistry/Biochemistry, CECD, University of Maryland, College Park, MD 20742, USA

impact energies for 50% probability of ignition or explosion are about 3.5 J (PETN), 6.3 J (RDX) and 38 J (TNT) [3]. (These correspond to 2.5 kg drop heights of 14, 26 and 155 cm, respectively.)

An interesting feature of PETN is that its detonation behavior has been observed to be direction-dependent within the crystal. Imposing shocks parallel to the [110] and [001] directions was found to lead to detonation, whereas parallel to the [101] and [100] did not [5–7]. Earlier work had already shown that the detonation velocities in the [110] and [001] directions differed, 8,887 versus 8,424 m/s, respectively [1].

In the context of these experimental observations, Kunz demonstrated computationally that the band gap in PETN decreased with pressure imposed in either the [001] or [100] directions, but to a greater extent for the former [8]. Taken in conjunction with Gilman's hypothesis that sensitivity is related to metallization of the solid [9], Kunz's results are consistent with direction-dependent detonation, as is also a molecular dynamics study of collision-induced PETN decomposition by Wu et al. [10].

Recently has been reported the preparation of Si-PETN, **4** [11], a silicon analog of PETN. This again involved treating the corresponding tetrol with nitric acid. A remarkable feature of Si-PETN is its extreme sensitivity: Impact is not necessary; just touching it with a spatula invariably produced an explosion!

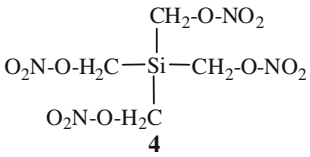

4

2 PETN and Si-PETN decomposition

The detonation of an energetic compound is believed to proceed through its decomposition [4, 12]. Accordingly, in an effort to understand why Si-PETN is so much more sensitive that even PETN, Liu et al. [13] have compared computationally several possible initial steps in PETN and Si-PETN decomposition.

In PETN, this is generally believed to begin with rupture of an O–NO_2 bond [10, 14–16], and Liu et al. did find this to be one of the two energetically preferred options, the other being HONO elimination. The corresponding processes for Si-PETN had barriers similar to those obtained for PETN, 35–40 kcal/mol.

Liu et al. [13] also examined the possibility of PETN, **1**, and Si-PETN, **4**, decomposition beginning via the rearrangement shown in Eq. 1, in which the linking oxygen interacts with the central carbon or silicon:

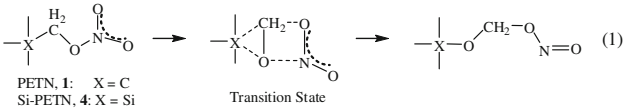

(1)

For PETN, the computed activation barrier for Eq. 1 was approximately double those for O–NO_2 bond cleavage and HONO elimination. For Si-PETN, however, it was 32 kcal/mol, less than for any of the other processes considered for either molecule; furthermore, the overall rearrangement was found to be quite exothermic, $\Delta H \sim -45$ kcal/mol [13].

The results of Liu et al. indicate that PETN decomposes via O–NO_2 cleavage and/or HONO elimination, whereas Si-PETN does so via Eq. 1. They concluded that the extreme sensitivity of Si-PETN can be attributed to (a) its relatively low energy requirement for Eq. 1, significantly less than for either of the likely initiating steps in PETN, and (b) the exothermicity of the Si-PETN rearrangement, which provides energy early in the decomposition that promotes its further progress and expansion [13].

Why does Eq. 1 occur so much more readily for Si-PETN than for PETN? Liu et al. [13] suggested that this is partly due to the greater size of the silicon atom compared to carbon, which facilitates, for the former, the enlargement of its coordination sphere from four to five in forming the transition state. While this argument is certainly reasonable, we would like to look at the activation process in greater detail. This will be done in terms of the reaction force concept, which shall now be briefly summarized.

3 The reaction force

The energetics of a chemical process are commonly depicted by the variation of the potential energy $V(\mathbf{R})$ of the system along an appropriate reaction coordinate $\mathbf{R}$. A typical profile of $V(\mathbf{R})$ for a one-step process A → B is presented in Fig. 1a; it shows the energies of the reactants, transition state and products. Considerable additional insight can be gained from $V(\mathbf{R})$ by taking its negative gradient along $\mathbf{R}$, which yields the classically defined reaction force $\mathbf{F}(\mathbf{R})$ (Fig. 1b) [17, 18].

$$\mathbf{F}(\mathbf{R}) = -\frac{\partial V(\mathbf{R})}{\partial \mathbf{R}} \tag{2}$$

$\mathbf{R}$ is normally taken to be the intrinsic reaction coordinate.

For the $V(\mathbf{R})$ in Fig. 1a, $\mathbf{F}(\mathbf{R})$ has a minimum at α and a maximum at γ, the inflection points of $V(\mathbf{R})$. These partition the reaction, in a rigorous manner that is dictated only

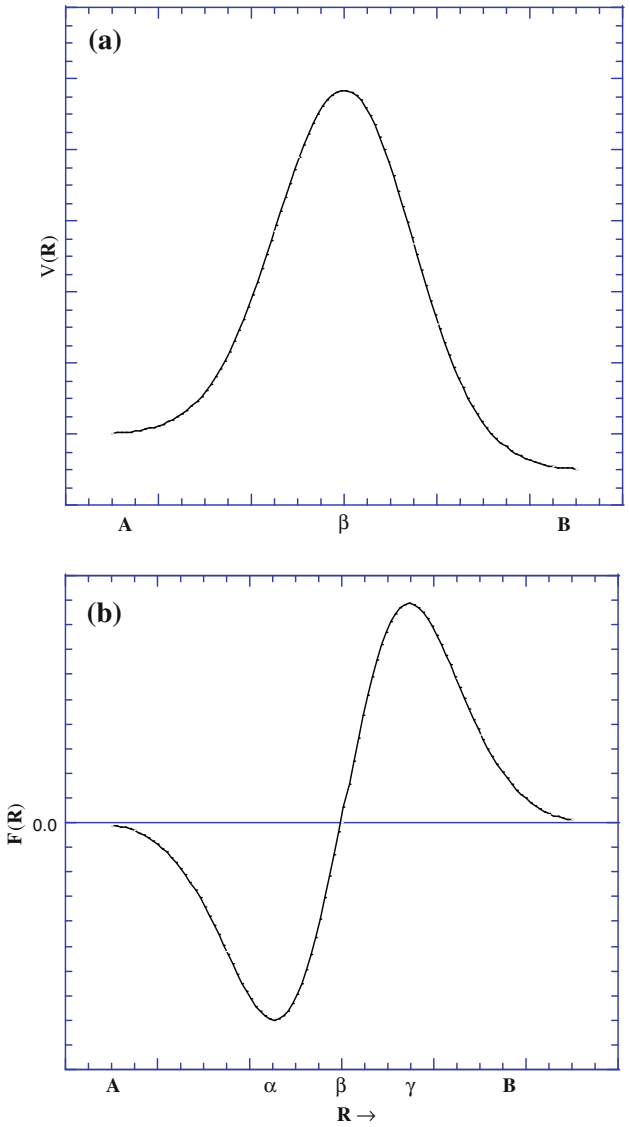

Fig. 1 Typical profiles of **a** the potential energy $V(\mathbf{R})$ and **b** the reaction force $\mathbf{F}(\mathbf{R})$, along the intrinsic reaction coordinate $\mathbf{R}$. The points $R = \alpha$ and $R = \gamma$ correspond to the minimum and the maximum of $\mathbf{F}(\mathbf{R})$; the transition state is at $R = \beta$. The zero of $\mathbf{F}(\mathbf{R})$ is indicated

by the form of $V(\mathbf{R})$, into three regions. The first is prior to the $\mathbf{F}(\mathbf{R})$ minimum, A → α, the second is between the minimum and maximum, $\alpha \rightarrow \gamma$, and the third is after the maximum, $\gamma \rightarrow$ B.

The general characteristics of these regions have been examined in a series of studies, which include S_N2 substitution [19–21], Markovnikov and anti-Markovnikov addition to a double bond [22], cycloaddition to olefins [23], bond dissociation [24–26], proton transfer [27–32] and nitro/*aci* tautomerization [33]. It was observed that the first region, A → α, is usually dominated by structural changes within the reactants, such as bond stretching, rotations and angle-bending. $\mathbf{F}(\mathbf{R})$ reflects the resistance to these changes, and is therefore increasingly retarding (i.e. negative) up to the point α, at which the system can generally be viewed as distorted states of the reactants. In the second region, $\alpha \rightarrow \gamma$, occurs the greatest part of the transition to products, emphasizing electronic factors: bonds breaking and new ones forming, rapid and extensive changes in properties such as electrostatic potentials and ionization energies, etc. All of this is manifested in a growing driving force; thus $\mathbf{F}(\mathbf{R})$ increases steadily until it reaches a maximum at γ, the end of the transition region. At this point, the system can often be regarded as distorted versions of the products. Between γ and B, these gradually relax to their final states. The three regions are commonly designated as reactant (A → α), transition ($\alpha \rightarrow \gamma$) and product ($\gamma \rightarrow$ B).

A key feature of the reaction force is that it shows the activation energy to be the sum of two components—the energies needed to go (a) from the reactants to the force minimum at α, and (b) from α to the transition state at β:

$$\begin{aligned}\Delta E_{\text{act}} &= V(\beta) - V(A) \\ &= [V(\beta) - V(\alpha)] + [V(\alpha) - V(A)] \\ &= \Delta E_{\text{act},2} + \Delta E_{\text{act},1}\end{aligned} \tag{3}$$

$\Delta E_{\text{act},1}$ is largely the energy required to overcome the system's resistance to the structural changes in the reactant region between A and α, while $\Delta E_{\text{act},2}$ supports the first portion of the transition to products, $\alpha \rightarrow \beta$.

This division of ΔE_{act} into its two components helps to explain how external agents, such as solvents and catalysts, affect reaction rates, i.e. whether they change mainly the structural ($A \rightarrow \alpha$) or the electronic ($\alpha \rightarrow \beta$) component of ΔE_{act} or both [20, 22, 32]. For example, in the S_N2 substitution $H_2O + CH_3Cl \rightarrow HCl + CH_3OH$, the effect of aqueous solution was found to be not upon the transition state but rather in promoting the initial C–Cl bond stretching [20]. In the keto-enol tautomerization of thymine, Mg(II) acting as a catalyst also affects the first (reactant) portion of the activation process (prior to the force minimum) [32]. On the other hand, in the addition of HCl to H_3C–CH=CH_2, chloroform solvent influences primarily the second part of the activation, $\alpha \rightarrow \beta$, approaching the transition state [22].

An additional insight into reaction mechanisms comes from the reaction force constant $\kappa(\mathbf{R})$, which is the second derivative of $V(\mathbf{R})$:

$$\kappa(\mathbf{R}) = \frac{\partial^2 V(\mathbf{R})}{\partial \mathbf{R}^2} = -\frac{\partial \mathbf{F}(\mathbf{R})}{\partial \mathbf{R}} \tag{4}$$

It follows from Eq. 4 that $\kappa(\mathbf{R})$ is negative throughout the entire transition region between α and γ [34, 35], in which $\mathbf{F}(\mathbf{R})$ is increasing. Transition state spectroscopy led

Zewail and Polanyi to conclude that a reaction has a continuum of transient, unstable configurations, a transition *region* rather than a single transition state [36, 37]. The reaction force constant $\kappa(\mathbf{R})$ reflects this continuum, and shows that it is bounded by the minimum and the maximum of $\mathbf{F}(\mathbf{R})$, at which $\kappa(\mathbf{R}) = 0$.

4 Approach

Our objective is to better understand why the rearrangement in Eq. 1 is so much favored for Si-PETN over PETN, both kinetically and thermodynamically. In order to simplify the computations, we have worked with the trimethyl mononitrate analogs of PETN and Si-PETN, i.e. **5** and **6**. Both of these are known and have been characterized [38]. The silicon compound is again by far the more sensitive; the impact energy (drop height) of **6** was reported as >1 J (>4 cm), compared to >100 J (>408 cm) for **5**. (The di- and trinitrate analogs have also been synthesized [38], and the silicon systems are similarly much more sensitive than the carbon ones.)

Table 1 Comparison of computed and experimental structures

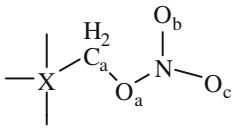

Distance (Å) or angle (°)	X=C			X=Si	
	1, PETN (X-ray)[a]	**5** (ED)[b]	**5** (calc)[c]	**6** (ED)[b]	**6** (calc)[c]
$X–C_a$	1.536	1.538	1.530	1.882	1.915
$C_a–O_a$	1.434	–	1.440	1.437	1.435
$O_a–N$	1.397	–	1.404	1.435	1.416
$N–O_b$	1.222	1.210[d]	1.203	1.206[d]	1.202
$N–O_c$	1.207	1.210[d]	1.195	1.206[d]	1.195
$X–C_a–O_a$	107.5	106.9	107.6	108.3	106.3
$C_a–O_a–N$	115.9	113.2	114.4	113.6	114.5
$O_b–N–O_c$	128.8	128.7	129.8	131.3	130.1

[a] Crystallographic data, Ref. [2]

[b] Electron diffraction data, Ref. [40]

[c] Present calculations, B3PW91/6-311G(d,p)

[d] Averages of $N–O_b$, $N–O_c$ distances

$(H_3C)_3C-CH_2ONO_2$ **5** $(H_3C)_3Si-CH_2ONO_2$ **6** $(H_3C)_3C-OCH_2ONO$ **7** $(H_3C)_3Si-OCH_2ONO$ **8**

The optimized geometries and the enthalpies along the intrinsic reaction coordinates for the rearrangements **5** → **7** and **6** → **8**, Eq. 1, were calculated at the density functional B3PW91/6-311G(d,p) level using Gaussian 03 [39]. In Table 1, our optimized geometries for **5** and **6** are compared to those obtained by electron diffraction [40] and also the molecular structure determined crystallographically for PETN [2]. Particularly pleasing is the good agreement with PETN, which provides some support for modeling Eq. 1 in terms of **5** and **6**. More will be forthcoming.

5 Reaction force analysis

In Table 2 are presented the computed structures, relative enthalpies at 298 K and key interatomic distances and angles at five points along the intrinsic reaction coordinate for the rearrangement **5** → **7**, Eq. 1; these points correspond to the ground state of **5**, the minimum of the reaction force at α, the transition state at β, the reaction force maximum at γ and the final rearrangement product **7**. Table 3 gives the same data for **6** → **8**. Table 4 summarizes the total activation enthalpy ΔH_{act} for each process, its two components $\Delta H_{act,1}$ and $\Delta H_{act,2}$ corresponding to the portions of the activation before and after the $\mathbf{F}(\mathbf{R})$ minimum, and finally the overall ΔH_{rxn}.

In terms of ΔH_{act} and ΔH_{rxn}, the rearrangements of **5** and **6** show exactly the same features as were found by Liu et al. [13] for PETN and Si-PETN. The activation barriers are relatively low for both silicon-containing molecules, 32–33 kcal/mol for Si-PETN and **6**, and more than twice as high for the carbon analogs. The reactions are quite exothermic for Si-PETN and **6**, with overall ΔH_{rxn} (298 K) of −40 to −45 kcal/mol, compared to just −10 to −14 kcal/mol for PETN and **5**. These similarities between PETN and **5** and between Si-PETN and **6** are reassuring with respect to using **5** and **6** to model PETN and Si-PETN.

To analyze why the activation barrier is so much smaller for **6** than for **5**, we first look at its components in each case, $\Delta H_{act,1}$ and $\Delta H_{act,2}$. Table 4 shows that the major difference in the activation energetics of **5** and **6** is in the initial portion of the process, in the reactant region prior to the $\mathbf{F}(\mathbf{R})$ minimum at α, which typically involves mainly structural changes. For **5**, these changes require 44.7 kcal/mol, compared to only 18.9 kcal/mol for **6**. Thus, 71% of the difference in the overall activation barriers reflects what is happening in the respective reactant regions.

Table 2 Computed structures, relative enthalpies at 298 K and some interatomic distances and angles at points along the intrinsic reaction coordinate for rearrangement $(H_3C)_3CC_aH_2O_aNO_bO_c$ (**5**) → $(H_3C)_3CO_aC_aH_2O_bNO_c$ (**7**), Eq. 1

	Reactant	Force min., α	Transition state, β	Force max, γ	Product
	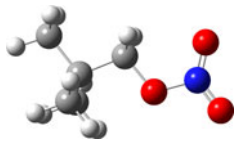	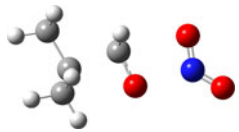	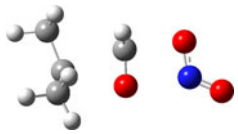	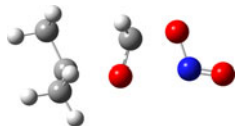	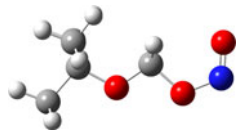
Relative H (298 K)	0.0	44.7	69.3	33.8	−9.7
Interatomic distances[a]					
$C–C_a$	1.530	1.807	2.243	2.496	2.416
$C–O_a$	2.397	2.344	2.213	1.908	1.446
$C_a–O_a$	1.440	1.316	1.270	1.343	1.381
$O_a–N$	1.404	2.049	2.212	2.396	3.492
$C_a–O_b$	2.566	2.445	2.064	1.635	1.437
$N–O_b$	1.203	1.189	1.248	1.364	1.374
$N–O_c$	1.195	1.198	1.203	1.179	1.183
Angles[a]					
$C–C_a–O_a$	107.6	96.0	72.2	49.1	32.1
$C–O_a–C_a$	37.5	50.0	74.7	98.8	117.4

Enthalpies are in kcal/mol, distances in Angstroms (Å) and angles in degrees. Colors of atoms: carbons are gray, hydrogens are white, nitrogen is blue and oxygens are red

[a] The symbol C refers only to the central carbons in **5**, the structures at positions α, β and γ, and **7**

Table 3 Computed structures, relative enthalpies at 298 K and some interatomic distances and angles at points along the intrinsic reaction coordinate for rearrangement $(H_3C)_3SiC_aH_2O_a$-NO_bO_c (**6**) → $(H_3C)_3SiO_aC_aH_2O_bNO_c$ (**8**), Eq. 1

	Reactant	Force min., α	Transition state, β	Force max, γ	Product
	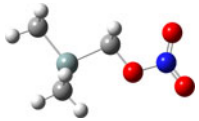	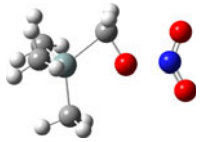	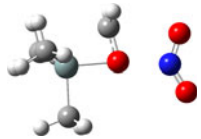	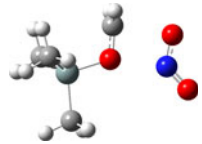	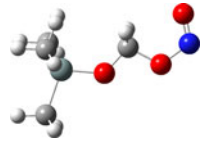
Relative H (298 K)	0.0	18.9	33.0	17.4	−40.0
Interatomic distances					
$Si–C_a$	1.915	1.976	2.136	2.513	2.746
$Si–O_a$	2.696	2.246	1.924	1.727	1.686
$C_a–O_a$	1.435	1.401	1.338	1.299	1.370
$O_a–N$	1.416	1.610	1.926	2.194	3.506
$C_a–O_b$	2.574	2.719	2.638	2.331	1.444
$N–O_b$	1.202	1.188	1.196	1.231	1.371
$N–O_c$	1.195	1.190	1.193	1.206	1.185
Angles					
$Si–C_a–O_a$	106.3	81.5	62.4	39.7	29.1
$Si–O_a–C_a$	43.0	60.5	79.6	111.5	127.6

Enthalpies are in kcal/mol, distances in Angstroms (Å) and angles in degrees. Colors of atoms: carbons are gray, silicon is blue-gray, hydrogens are white, nitrogen is blue and oxygens are red

Table 4 Computed activation enthalpies ΔH_{act}, their components $\Delta H_{act,1}$ and $\Delta H_{act,2}$, and the overall enthalpy of reaction, ΔH_{rxn}, for the reactions shown in Eq. 1, at 298 K

Reaction	$\Delta H_{act,1}$	$\Delta H_{act,2}$	ΔH_{act}	ΔH_{rxn}
$(H_3C)_3CC_aH_2O_aNO_bO_c$ (**5**) → $(H_3C)_3CO_aC_aH_2O_bNO_c$ (**7**)	44.7	24.6	69.3	−9.7
$(H_3C)_3SiC_aH_2O_aNO_bO_c$ (**6**) → $(H_3C)_3SiO_aC_aH_2O_bNO_c$ (**8**)	18.9	14.1	33.0	−40.0

Values are in kcal/mol. Computational level: B3PW91/6-311G(d,p)

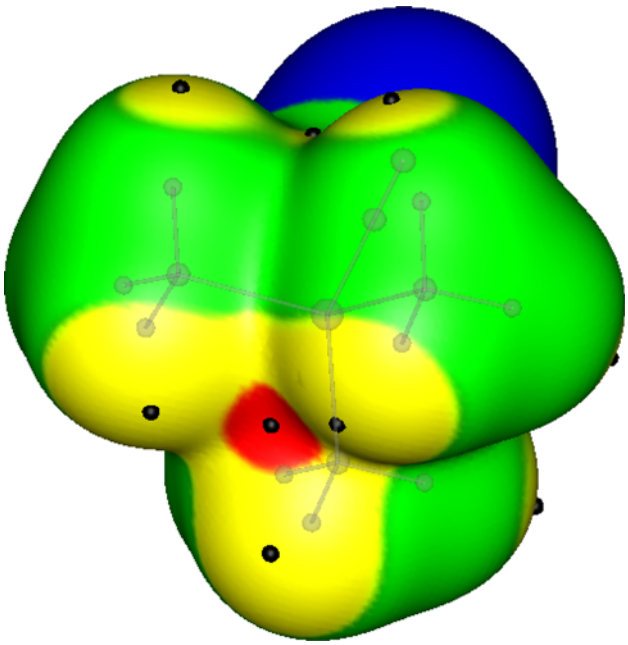

Fig. 2 Computed electrostatic potential on the 0.001 au molecular surface of $(H_3C)_3Si$–CN. The three methyl groups face the reader; the CN is pointing into the paper, the nitrogen being visible (*blue*) at the *top*. Color ranges, in kcal/mol, are: *blue* <0.0 (negative), *green* between 0.0 and 14.1, *yellow* between 14.1 and 21.3, *red* >21.3. *Black circles* indicate local surface maxima. The most positive is a positive σ–hole (*red*), of magnitude 25.7 kcal/mol, induced on the silicon by the strongly electron-withdrawing CN group, on the extension of the NC–Si bond. One of the σ–holes on the extensions of the H_3C–Si bonds, 15.1 kcal/mol, is in the *upper central* part of the figure. Next to both of the σ–holes shown are local maxima of 15.8–20.0 kcal/mol due to methyl hydrogens

What is it that is happening? Tables 2 and 3 show a variety of structural effects for both **5** and **6** in the regions before the **F**(**R**) minima. For **5**, the dominant ones are the stretching of two bonds: the C–C_a by 0.277 Å and the O_a–N by fully 0.645 Å. This requires energy. In **6**, on the other hand, the Si–C_a and O_a–N bonds lengthen by only 0.061 and 0.194 Å in the reactant region. What is important here for **6** is that the nonbonded Si and O_a atoms move closer to each other by 0.450 Å. This is reflected in the Si–C_a–O_a angle decreasing by 24.8°. The approach of O_a to Si, which will lead eventually to the formation of the Si–O_a bond, should already be accompanied by a significant release of energy, given the strengths of Si–O bonds (see [41], and also the next section of this paper). Thus, **6** needs less energy than **5** in the reactant region (before α) because (a) it is undergoing less bond stretching, and (b) it is benefiting from the favorable Si · · · O_a interaction.

In the second portion of the activation process of **5**, between the **F**(**R**) minimum at α and the transition state at β, the C–C_a and O_a–N bonds start to break and C and O_a begin to bond, as do C_a and O_b. The latter interactions bring $\Delta H_{act,2}$ down to 24.6 kcal/mole for **5**. However, **6** again requires less energy. Between α and β, the breaking of the Si–C_a and O_a–N bonds in **6** proceeds rather slowly, while Si and O_a come closer by another 0.322 Å and the Si–C_a–O_a angle is reduced by 19.1°, taking a big step toward Si–O_a bond formation. Thus, $\Delta H_{act,2}$ is also less for **6** than for **5** (Table 4), although not nearly by as much as $\Delta H_{act,1}$.

The difference in the activation barriers of **5** and **6** can therefore be attributed to their contrasting pathways from reactant → α → transition state: **5** begins with energy-consuming bond stretchings and then breakings, largely delaying energy-releasing bond formation until after the transition state. The silicon analog **6**, on the other hand, is slower to begin the energy-demanding steps, but starts right away to benefit from the eventual formation of a strong Si–O bond.

As suggested by Liu et al. [13] for Si-PETN, one factor in the O_a in **6** being able to immediately move toward the silicon is the size of the latter atom, which allows it to accommodate the approaching oxygen while essentially maintaining four covalent bonds. The relatively small central carbon in **5**, on the other hand, must make room for O_a by C_a moving out of the way. But what is the driving force for the approach of O_a to Si? We believe that it is the presence of a favorable Si · · · O_a interaction already in the ground state of **6**. Indeed, short Si · · · O_a contacts have been found crystallographically in the dinitrate analog of **6** [38, 40]. Mitzel et al. have observed unexpectedly small intramolecular 1,3 Si–N and Si–O distances and Si–Z–N and Si–Z–O angles in molecules such as $ClH_2SiON(CH_3)_2$, $(F_3C)F_2SiON(CH_3)_2$, and $H_3SiN(CH_3)OCH_3$ [42–44].

The origin of the Si · · · O_a interaction in **6**, as well as those observed by Mitzel et al., can readily be explained. When Group IV–VII atoms form covalent bonds, the outer (non-involved) lobe of the bonding orbital undergoes a depletion

in electronic density. This has been labeled a σ–hole [45–47]. If the depletion is sufficiently great, there results a region of positive electrostatic potential with a local surface maximum. σ–Holes become more positive, and the resulting interactions stronger, for the more polarizable, i.e. larger atoms in a Group, and usually as the remainder of the molecule becomes more electron-withdrawing [46–49].

As an example, in Fig. 2 is displayed the electrostatic potential on the molecular surface of $Si(CH_3)_3CN$, computed using the WFA Surface Analysis Suite [50]. The surface is taken to be the 0.001 au (electrons/Bohr^3) contour of the electronic density, as proposed by Bader et al. [51]. There are four positive σ–holes on the silicon surface, each corresponding to a local maximum of the electrostatic potential. The largest in magnitude is 25.7 kcal/mol on the extension of the bond from the strongly electron-withdrawing CN group; the others are 15.1 kcal/mol, on the extensions of the H_3C–Si bonds. The methyl hydrogens are also positive, with local maxima ranging from 15.8 to 20.0 kcal/mol.

A positive σ–hole can interact electrostatically with a negative site (such as O_a of **6**), either inter- or intramolecularly. There is a great deal of evidence, both experimental [52–59] and computational [45–49, 60–62], attesting to the significance of such interactions. (They are called "halogen bonds" when the σ–hole is on a halogen atom.) Very recently, complex formation between SiF_4 and di- and triamines has been interpreted in terms of electrostatic interactions between the lone pairs of the amine nitrogens and the Si σ–holes induced by the four F–Si bonds [62].

We have also computed the molecular surface electrostatic potential of **6**, which should intrinsically be quite similar to that shown for $Si(CH_3)_3CN$ in Fig. 2. However, three of the four local maxima on the silicon in **6** are masked; one of the three σ–holes on the extensions of the H_3C–Si bonds is involved in the Si $\cdots$ O_a intramolecular interaction, and the other two are difficult to distinguish because of the long and bulky $-CH_2-ONO_2$ group. We are accordingly not showing the surface potential plot of **6**. The only silicon σ–hole in **6** that would clearly be seen is the strongest, 18.0 kcal/mol, on the extension of the bond from the electron-withdrawing $-CH_2-ONO_2$ group. There are also local maxima on the methyl hydrogens of **6**.

The driving force for the approach of O_a to Si in **6** is the interaction between O_a and (a) a silicon σ–hole along the extension of an H_3C–Si bond, analogous to that seen in Fig. 2, and (b) the neighboring methyl hydrogens. The corresponding interaction is much weaker in **5**, for which we found that the central carbon, being less polarizable than silicon, has no positive σ–holes whatsoever. The strength of this interaction in **6**, and the fact that the size of the silicon atom allows it to proceed without prior stretching of other bonds, explain the low energy requirement for reaching the force minimum ($\Delta H_{act,1}$ of 18.9 kcal/mol for **6** vs. 44.7 kcal/mol for **5**).

6 Exothermicities of rearrangements

Liu et al. [13] ascribed the much greater exothermicity of the Si-PETN rearrangement to the strength of the Si–O bond that is formed. We can provide some quantitative support for this explanation.

If one looks only at the bonds broken and formed in the rearrangements of **5** and **6**, the differences between the two processes are breaking C–C_a versus Si–C_a and forming C–O_a versus Si–O_a. The former two bonds tend to have roughly similar dissociation enthalpies [41]; thus, as a very crude approximation, it could be suggested that the difference in the overall ΔH_{rxn} of the two rearrangements can be estimated by comparing the ΔH for forming the C–O_a and Si–O_a bonds in **7** and **8**. Since Si–O bond enthalpies, while generally larger in magnitude, tend to be quite variable [41], we have computed ΔH for the formation of the C–O_a bond in **7** and the Si–O_a bond in **8**. The was done at the B3PW91/6-31++G(3d,2p) level, using B3PW91/6-311G(d,p) optimized geometries.

The results are:

$$(H_3C)_3C\cdot + \cdot OCH_2ONO \rightarrow \mathbf{7}$$
$$\Delta H\ (298\,K) = -79.5\,kcal/mol \quad (5)$$

$$(H_3C)_3Si\cdot + \cdot OCH_2ONO \rightarrow \mathbf{8}$$
$$\Delta H\ (298\,K) = -112.7\,kcal/mol \quad (6)$$

Taking the difference as a measure of the relative exothermicities of the rearrangements of **5** and **6**, we have that of **6** being more exothermic by 33.2 kcal/mol. This is, perhaps fortuitously, quite close to the 30.3 kcal/mol difference between the computed ΔH_{rxn} in Table 4.

7 Discussion and summary

Our objective in this investigation has been to better understand why the rearrangement in Eq. 1 is so much more (a) facile and (b) exothermic for Si-PETN than for PETN. We used **5** and **6** as models for PETN and Si-PETN, which seems justified because **5** and **6** have nearly the same relative activation barriers and exothermicities for Eq. 1 as do PETN and Si-PETN.

Reaction force analysis shows that most of the difference in the activation energies of **5** and **6** reflects the greater ease with which **6** reaches the **F**(**R**) minimum at α; it requires only 18.9 kcal/mol in this first (reactant) region versus 44.7 kcal/mol for **5**. This is because the size of the silicon atom permits **6** to immediately benefit from an

energy-releasing intramolecular electrostatic interaction between O_a and a positive σ–hole on the silicon plus the surrounding methyl hydrogens. The corresponding interaction in **5** is not nearly as strong because we found the central carbon to lack positive σ–holes; furthermore, the approach of O_a has to be delayed until after C_a has moved away.

We propose that analogous interactions between linking oxygens and silicon positive σ–holes are occurring in Si-PETN. There are no methyl hydrogens involved, but the silicon σ–holes in Si-PETN should be more positive because the silicon is bonded to four electron-withdrawing $–CH_2–ONO_2$ groups, rather than one as in **6**. For example, whereas the local maximum potential induced by the single $–CH_2–ONO_2$ in **6** is 18.0 kcal/mol, we found the two in the dinitrate silicon analog to each be 30.6 kcal/mol. The much lower activation barrier for Si-PETN than for PETN in Eq. 1 can therefore be explained in terms of the $Si\cdots O_a$ interaction in conjunction with the large size of silicon that allows it to progress without delay toward $Si–O_a$ bond formation.

If at least one $–CH_2–ONO_2$ group in Si-PETN undergoes the rearrangement in Eq. 1, a significant amount of energy is produced. This has been rationalized on the basis of the strength of the Si–O bond that is created (Sect. 6 and [13]). This energy is more than enough to allow a second $–CH_2–ONO_2$ to overcome the barrier to rearrangement. However, it might also be used for further steps involving the rearranged group. To examine this possibility, we computed the dissociation enthalpies of the $OCH_2–ONO$ and the O–NO bonds in **8**, which is the rearranged form of **6**. The B3PW91/6-31++G(3d,2p)//B3PW91/6-311G(d,p) procedure was again utilized. The results are:

$$\mathbf{8} \rightarrow (H_3C)_3Si-O(H_2)C\cdot + \cdot ONO \qquad \Delta H\ (298\,K) = 49.7\,\text{kcal/mol} \tag{7}$$

$$\mathbf{8} \rightarrow (H_3C)_3Si-OCH_2O\cdot + \cdot NO \qquad \Delta H\ (298\,K) = 32.7\,\text{kcal/mol} \tag{8}$$

The second of these is less than the exothermicity of the rearrangement of **6**, and could well be a follow-up step in the decomposition. This remains to be investigated.

Acknowledgments We thank Dr. Felipe A. Bulat for his help and expertise in preparing Fig. 2 and for many useful discussions. JSM, PL and PP appreciate the support of the Defense Threat Reduction Agency, Contract No. HDTRA1-07-1-0002, Project Office Dr. William Wilson. Financial support (to TMK) of this work by LMU and the U.S. Army Research Laboratory (ARL) under Contract No. W911NF-09-2-0018 is gratefully acknowledged.

References

1. Urbański T (1984) Chemistry and technology of explosives, vol 4. Pergamon Press, Oxford
2. Cady HH, Larson AC (1975) Acta Cryst B31:1864–1869
3. Gibbs TR, Popolato A (eds) (1980) LASL explosive property data. University of California Press, Berkeley
4. Meyer R, Köhler J, Homburg A (2007) Explosives, 6th edn. Wiley-VCH, Weinheim
5. Dick JJ (1984) Appl Phys Lett 44:859–860
6. Dick JJ (1997) J Appl Phys 81:601–612
7. Yoo C-S, Holmes NC, Souers PC, Wu CJ, Ree FH, Dick JJ (2000) J Appl Phys 88:70–75
8. Kunz AB (1996) Mater Res Soc Symp Proc 418:287–292
9. Gilman JJ (1993) Philos Mag B67:207
10. Wu CJ, Ree FH, Yoo C-S (2004) Propellants Explos Pyrotech 29:296–303
11. Klapötke TM, Krumm B, Ilg R, Troegel D, Tacke R (2007) J Am Chem Soc 129:6908–6915
12. Politzer P, Murray JS (eds) (2003) Energetic materials. Part 1. Decomposition, crystal and molecular properties. Part 2. Detonation, combustion. Elsevier, Amsterdam
13. Liu W-G, Zybin SV, Dasgupta S, Klapötke TM, Goddard WA III (2009) J Am Chem Soc 131:7490–7491
14. Hauser HM, Field JE, Mohan VK (1983) Chem Phys Lett 99:66–70
15. Hiskey MA, Brower KR, Oxley JC (1991) J Phys Chem 95:3955–3960
16. Oxley JC (2003) In: Politzer P, Murray JS (eds) Energetic materials. Part I. Decomposition, crystal and molecular properties, chap 1. Elsevier, Amsterdam
17. Toro-Labbé A, Gutiérrez-Oliva S, Murray JS, Politzer P (2007) Mol Phys 105:2619–2625
18. Toro-Labbé A, Gutiérrez-Oliva S, Politzer P, Murray JS (2008) In: Chattaraj P (ed) Theory of chemical reactivity, chap 21. Taylor & Francis, Boca Raton
19. Politzer P, Burda JV, Concha MC, Lane P, Murray JS (2006) J Phys Chem A 110:756–761
20. Burda JV, Toro-Labbé A, Gutiérrez-Oliva S, Murray JS, Politzer P (2007) J Phys Chem A 111:2455–2458
21. Echegaray E, Toro-Labbé A (2008) J Phys Chem A 112:11801–11807
22. Burda JV, Murray JS, Toro-Labbé A, Gutiérrez-Oliva S, Politzer P (2009) J Phys Chem A 113:6500–6505
23. Jaque P, Toro-Labbé A, Geerlings P, De Proft F (2009) J Phys Chem A 113:332–344
24. Politzer P, Murray JS, Lane P, Toro-Labbé A (2007) Int J Quantum Chem 107:2153–2157
25. Politzer P, Murray JS (2008) Collect Czechoslov Chem Commun 73:822–830
26. Murray JS, Toro-Labbé A, Clark T, Politzer P (2009) J Mol Model 15:701–706
27. Toro-Labbé A, Gutiérrez-Oliva S, Concha MC, Murray JS, Politzer P (2004) J Chem Phys 121:4570–4576
28. Herrera B, Toro-Labbé A (2004) J Chem Phys 121:7096–7102
29. Politzer P, Toro-Labbé A, Gutiérrez-Oliva S, Herrera B, Jaque P, Concha MC, Murray JS (2005) J Chem Sci 117:467–472
30. Gutiérrez-Oliva S, Herrera B, Toro-Labbé A, Chermette H (2005) J Phys Chem A 109:1748–1751
31. Rincón E, Jaque P, Toro-Labbé A (2006) J Phys Chem A 110:9478–9485
32. Herrera B, Toro-Labbé A (2007) J Phys Chem A 111:5921–5926
33. Murray JS, Lane P, Göbel M, Klapötke TM, Politzer P (2009) Theor Chem Acc 124:355–363
34. Jaque P, Toro-Labbé A, Politzer P, Geerlings P (2008) Chem Phys Lett 456:135–140
35. Toro-Labbé A, Gutiérrez-Oliva S, Murray JS, Politzer P (2009) J Mol Model 15:707–710
36. Polanyi JC, Zewail AH (1995) Acc Chem Res 28:119–132
37. Zewail AH (2000) J Phys Chem A 104:5660–5694

38. Klapötke TM, Krumm B, Nieder A, Tacke R, Troegel D (2009) New trends in research of energetic materials, part 1. Institute of Energetic Materials, University of Pardubice, Czech Republic, pp 262–276
39. Frisch MJ, Trucks GW, Schlegel HB, Scuseria GE, Robb MA, Cheeseman JR, Montgomery JA Jr, Vreven T, Kudin KN, Burant JC, Millam JM, Iyengar SS, Tomasi J, Barone V, Mennucci B, Cossi M, Scalmani G, Rega N, Petersson GA, Nakatsuji H, Hada M, Ehara M, Toyota K, Fukuda R, Hasegawa J, Ishida M, Nakajima T, Honda Y, Kitao O, Nakai H, Klene M, Li X, Knox JE, Hratchian HP, Cross JB, Bakken V, Adamo C, Jaramillo J, Gomperts R, Stratmann RE, Yazyev O, Austin AJ, Cammi R, Pomelli C, Ochterski JW, Ayala PY, Morokuma K, Voth GA, Salvador P, Dannenberg JJ, Zakrzewski VG, Dapprich S, Daniels AD, Strain MC, Farkas O, Malick DK, Rabuck AD, Raghavachari K, Foresman JB, Ortiz JV, Cui Q, Baboul AG, Clifford S, Cioslowski J, Stefanov BB, Liu G, Liashenko A, Piskorz P, Komaromi I, Martin RL, Fox DJ, Keith T, Al-Laham MA, Peng CY, Nanayakkara A, Challacombe M, Gill PMW, Johnson B, Chen W, Wong MW, Gonzalez C, Pople JA (2004) Gaussian 03, revision E.01. Gaussian, Inc., Wallingford
40. Evangelisti C, Klapötke TM, Krumm B, Nieder A, Berger RJF, Hayes SA, Mitzel NW, Troegel D, Tacke R (submitted)
41. Luo Y-R (2007) Comprehensive handbook of chemical bond energies. CRC Press, Taylor & Francis, Boca Raton
42. Mitzel NW, Losehand U (1998) J Am Chem Soc 120:7320–7327
43. Mitzel NW, Oberhammer H (1998) Inorg Chem 37:3593–3598
44. Mitzel NW, Vojinović K, Fröhlich R, Foerster T, Robertson HE, Borisenko KB, Rankin DWH (2005) J Am Chem Soc 127:13705–13713
45. Clark T, Hennemann M, Murray JS, Politzer P (2007) J Mol Model 13:291–296
46. Politzer P, Lane P, Concha MC, Ma Y, Murray JS (2007) J Mol Model 13:305–311
47. Murray JS, Lane P, Politzer P (2009) J Mol Model 15:723–729
48. Murray JS, Lane P, Politzer P (2008) Int J Quantum Chem 108:2770–2781
49. Riley KE, Murray JS, Concha MC, Politzer P, Hobza P (2009) J Chem Theory Comput 5:155–163
50. Bulat FA, Toro-Labbé A, Brinck T, Murray JS, Politzer P (2010) J Mol Model (in press)
51. Bader RFW, Carroll MT, Cheeseman JR, Chang C (1987) J Am Chem Soc 109:7968–7979
52. Di Paolo T, Sandorfy C (1974) Can J Chem 52:3612–3622
53. Rosenfeld RE Jr, Parthasarathy R, Dunitz JD (1977) J Am Chem Soc 99:4860–4862
54. Ramasabbu N, Parthasarathy R, Murray-Rust P (1986) J Am Chem Soc 108:4308–4314
55. Burling FT, Goldstein BM (1992) J Am Chem Soc 114:2313
56. Auffinger P, Hays FA, Westhof E, Shing Ho P (2004) Proc Natl Acad Sci USA 101:16789–16794
57. Metrangolo P, Neukirsch H, Pilati T, Resnati G (2005) Acc Chem Res 38:386–395
58. Cheng F, Hector AL, Levason W, Reid G, Webster M, Zhang Z (2009) Chem Commun 1334–1336
59. Hassan AEA, Sheng J, Jiang J, Zhang W, Huang Z (2009) Org Lett 11:2503–2506
60. Bleiholder C, Werz DB, Köppel H, Gleiter R (2006) J Am Chem Soc 128:2666
61. Clark T, Murray JS, Lane P, Politzer P (2008) J Mol Model 14:689–697
62. Politzer P, Murray JS, Lane P, Concha MC (2009) Int J Quantum Chem 109:3773–3780